Journal of Zhejiang University-SCIENCE A 2026 27(5):493-505
www.jzus.zju.edu.cn; www.springer.com/journal/11582
E-mail: jzus_a@zju.edu.cn

Research Article
https://doi.org/10.1631/jzus.A2500604

Check for updates

Flow analysis of asymmetric clearance and optimization of pressure equalization grooves to mitigate hydraulic spool valve sticking

Zhen-hao LIN[1,2], Yu-wei WANG[1], Zhe-hui MA[1], Tian-xiao ZHANG[1], Zhi-jiang JIN[1,3], Jin-yuan QIAN[1]✉

[1]*Institute of Advanced Equipment, College of Energy Engineering, Zhejiang University, Hangzhou 310027, China*
[2]*Hangzhou Valvever Intelligent Technology Co., Ltd., Hangzhou 310058, China*
[3]*Institute of Wenzhou, Zhejiang University, Wenzhou 325036, China*

Abstract: The hydraulic spool valve is a critical control component in aerospace hydraulic systems. However, complex working environments can cause the valve core to become stuck, thus severely restricting the performance of such valves. This in turn can hinder the precise control of hydraulic oil, reduce the stability of the hydraulic system, and lead to serious accidents in aerospace systems. The unbalanced radial force and solid particle intrusion into the fit clearance are the main factors behind this sticking. To better understand these issues, in this study, we simulated the fluid dynamics and particle behavior within the clearance of the valve core and analyzed the effects of inclination angle, clearance size, particle diameter, and pressure equalization groove (PEG) properties. The mechanism behind valve core sticking was revealed, and it was found that the PEG has an inhibitory effect on the unbalanced radial force and particle intrusion. Furthermore, we proposed an optimized structure for a triangular pressure equalization groove with an arc-shaped bottom (Tri-PEG). The structural parameters were determined through multi-objective optimization, with the objectives of minimizing the leakage at the clearance and maximizing the particle volume fraction at the bottom of the Tri-PEG. The optimal parameters were an arc-shaped radius of 0.200 mm, a groove depth of 0.392 mm, and a half groove width of 0.215 mm. Comparing Tri-PEG with a rectangular PEG, the leakage was reduced by 12%, and the particle concentration was increased by 6%. Overall, these findings serve as an important reference for alleviating spool valve sticking.

Key words: Spool valve; Flow characteristics; Multi-objective optimization; Solid–liquid two-phase flow; Aerospace hydraulic systems; Valve sticking

1 Introduction

Hydraulic systems serve as fundamental subsystems in aerospace applications, supporting various safety-critical operations (Shanbhag et al., 2021; Deng et al., 2023; Hou et al., 2025). Hydraulic spool valves, being common control components in hydraulic systems, play an important role in controlling the flow rate (Jiang et al., 2019; Lu et al., 2022), pressure (Zhong et al., 2021), and flow direction (Zhao et al., 2021) in such systems (Li et al., 2023). Accordingly, faults in hydraulic spool valves can cause serious problems and accidents (Li et al., 2025). In particular, valve core sticking may lead to performance degradation and function maladjustment (Chu et al., 2021; Sun et al., 2026); this is one of the most common faults in hydraulic systems (Wang et al., 2023). Suppression or resolution of this problem is thus vital for improving the safety and stability of aerospace hydraulic systems (Qian et al., 2023; Zhu et al., 2026).

Valve core sticking is the phenomenon of increased resistance and delayed response of the valve core during movement (Li et al., 2014). The increased resistance is due to the sticking force. For hydraulic spool valves, the main causes of valve core sticking are the unbalanced radial force (Zhang et al., 2024) and solid particle contamination (Yin et al., 2017; Liu et al., 2020; Chen et al., 2024).

✉ Jin-yuan QIAN, qianjy@zju.edu.cn
Zhen-hao LIN, https://orcid.org/0000-0003-3040-7656
Yu-wei WANG, https://orcid.org/0009-0000-7935-4765
Zhe-hui MA, https://orcid.org/0009-0008-9552-4873
Zhi-jiang JIN, https://orcid.org/0000-0002-8063-709X
Jin-yuan QIAN, https://orcid.org/0000-0002-5438-0833

Received Nov. 17, 2025; Revision accepted Jan. 7, 2026;
Crosschecked Mar. 25, 2026; Online first May 16, 2026

The unbalanced radial force on the surface of the valve core is caused by chaotic turbulent flow of the fluid (Zhang YH et al., 2025). The fluid boundary in the valve is formed by the valve body and internal components; this boundary is asymmetric and complex. Thus, analytical calculation of the unbalanced radial force is difficult. A multitude of numerical simulation studies have been conducted to analyze the factors influencing the unbalanced force. For instance, Gao et al. (2020) analyzed the torque of the butterfly plates of flip check valves and swing check valves. Under fully-open conditions, the former was 53.86% of the latter, which is also the reason why flip-check valves are prone to vibration. Also, Qian et al. (2016, 2021) analyzed the formation mechanism of unbalanced force on the bottom surface of piston-type valve cores. Their results indicated that due to the curvature of the inlet flow channel, the inlet fluid formed an impact on the bottom surface of the valve core. This caused the pressure on the bottom surface of the valve core near the inlet to be lower than that near the outlet, resulting in an unbalanced torque and tilting of the valve core. Moreover, Lisowski et al. (2018) studied the fluid force on the core of a proportional control valve during the initial stage of spool opening. They found that a single incision can enable the valve to operate at very low flow rates, and there is significant radial hydraulic asymmetry.

During the processing and assembly of hydraulic spool valves, inevitable problems arise, such as eccentricity, reverse coning, inclination, and end protrusion. These problems can lead to asymmetric fit clearance between the valve core and the valve body. In asymmetric fit clearance, the pressure drop is large at positions with small clearance and is small at positions with large clearance. This results in an uneven pressure difference on the surface of the valve core (Fig. S1 of the electronic supplementary materials (ESM)).

When solid particles from outside the valve, or those generated by corrosion and wear of valve components, are mixed into the fluid, these solid particles enter the clearance between the valve core and other components with the fluid. When solid particles, the valve core, and other components are in contact with each other, the resistance of the valve core increases. This can cause the valve core to become stuck or jammed (Zhang J et al., 2025). It may even threaten the stability and safety of the entire system (Sun et al., 2021). Therefore, it is crucial to analyze the flow characteristics of solid particles and reveal their patterns of motion. With this in mind, Terrell and Higgs III (2007) proposed a kinematic trajectory model for predicting material wear particles; their predicted results were compared with experimental data and shown to be accurate. Also, Mittal and Iaccarino (2005) simulated the flow of pollutant particles in the fitting clearance based on the submerged boundary method, solving the problem of submerged solid boundary flow. Furthermore, Domagała et al. (2018) constructed collision angle and velocity models for particles of different materials inside the spool valve. This model was used to predict the motion of particles inside the valve body.

In hydraulic spool valves, when unbalanced radial forces and solid particles both exert influence, they can cause coupling sticking issues (Fig. S2 of the ESM). The unbalanced radial force causes the valve core to tilt, resulting in an asymmetric fit clearance. The reduction in clearance and the invasion of solid particles together led to the sticking of the valve core.

Numerous studies have focused on preventing control valve core sticking and optimizing valve core designs. For instance, Amirante et al. (2016) reduced the hydraulic force on the valve core by designing a central conical surface and side structure of the valve core. Also, Zhang et al. (2020) analyzed the flow characteristics of coupled throttling channels. A neural network and genetic algorithm were used to optimize the design of the throttling groove structure, with the goal of evaluating the throttling stiffness for flow stability. Moreover, Gui et al. (2022) conducted optimization analysis on the valve core structure using the optimal non-dominated sorting genetic algorithm II (NSGA-II). Their results showed that the optimized hydraulic force was significantly reduced, and the piezoelectric servo valve had good response performance.

Many scholars have proposed asymmetric pressure equalization groove (PEG) structures to reduce the hydraulic force of the valve core in the fitting clearance. For example, Hong and Kim (2016) proposed a spiral PEG structure and compared its performance with typical PEGs. It was found that valve cores with spiral grooves are more likely to alleviate the situation of uneven pressure distribution around the valve core. Additionally, Zheng et al. (2020) proposed a composite groove structure consisting of an annular PEG and a spiral PEG. The flow characteristics of the composite groove piston were analyzed from the aspects of pressure distribution, tilting torque, clearance

leakage, pressure balance, and clearance flow rate. The above two types of groove structures can effectively reduce the upper and lower pressure differences of the valve core. However, due to the connected state between adjacent PEGs, when the end of the valve core does not coincide with the valve body, it may cause significant leakage; therefore, this is unsuitable in some situations.

Although numerous studies have been conducted to investigate valve core sticking in control valves and associated sticking suppression methods, there are still limitations in current mechanisms of valve core sticking as well as optimized designs of valve cores. Furthermore, studies on valve core sticking under the coupled effect of unbalanced radial force and solid particles are still relatively limited. Meanwhile, there is sparse research on valve core optimization considering multiple target quantities.

To address these limitations, we analyze the fluid dynamics and particle behavior within the fit clearance of a hydraulic spool valve under different inclination angles, clearance sizes, and particle diameters. Moreover, we introduce a triangular PEG with an arc-shaped bottom (Tri-PEG) and optimize its structural parameters to achieve a balance between reducing leakage rate and lessening solid particle aggregation.

2 Methods

2.1 Physical model

The hydraulic spool valve is mainly composed of the driving component, valve body, valve sleeve, and valve core, as shown in Fig. 1. At the position marked by the red frame, the valve core and the sleeve can easily come into contact. We assume that there is no eccentricity resulting from the assembly of the valve core, valve body, and valve sleeve and that the valve core has no reverse coning or burrs from processing. We establish a model for the fit clearance after the valve core shoulder is tilted, including the clearance flow channel models without and with PEGs, as depicted in Figs. 1b and 1c, respectively. The distance from the shoulder end face of the valve core to the center of mass (a) is 19.0 mm. The length of valve core shoulder (l) is 9.2 mm. The inclination angles are γ=0.01°, 0.03°, and 0.05°, and the initial values of the clearance between components are δ=15, 20, and 25 μm. When the clearance is 10 μm or less, due to the inclination angle, the minimum gap may be smaller than the particle diameter. The valve core will then experience severe mechanical jamming, so the flow characteristics and force analysis will have no research significance.

2.2 Numerical methods

In this study, hydraulic oil containing solid particles was used as the medium for numerical modeling. The fluid phase and solid phase were assumed to be continuous fluids. An Euler–Euler solid–liquid two-phase flow model was adopted, which is commonly used to solve multi-phase flow problems with interactions between phases (Shi et al., 2024). Compared with a mixed model, this model has higher calculation accuracy. In the Euler–Euler model, each phase satisfies the continuity equation and the momentum equation. The continuity equation for the k phase is as follows:

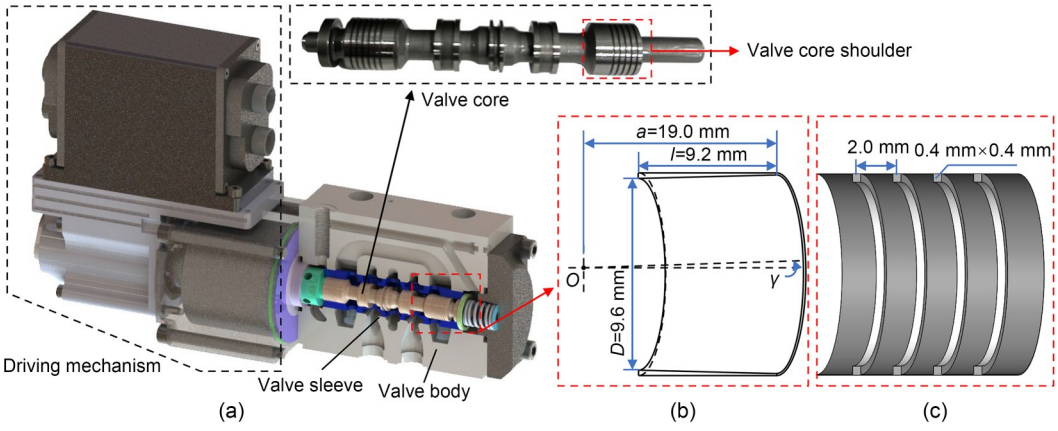

Fig. 1 Hydraulic spool valve and flow channel of the fit clearance: (a) hydraulic spool valve; (b) clearance flow channel model without PEGs; (c) clearance flow channel model with PEGs

$$\frac{\partial}{\partial t}(\alpha_k\rho_k)+\nabla\cdot(\alpha_k\rho_k\boldsymbol{v}_k)=\sum(\dot{m}_{pk}-\dot{m}_{kp}), \quad (1)$$

where $\boldsymbol{v}_k$ is the velocity of the k phase, $\dot{m}_{pk}$ is the derivation of mass transfer from the k to p phases, $\dot{m}_{kp}$ is the derivative of mass transfer from the p to k phases, t is the time, α_k is the volume ration of the k phase, and ρ_k is the density of the k phase.

The momentum equation of the k phase is as follows:

$$\begin{aligned}\frac{\partial}{\partial t}(\alpha_k\rho_k\boldsymbol{v}_k)+\nabla\cdot(\alpha_k\rho_k\boldsymbol{v}_k\boldsymbol{v}_k)=&-\alpha_k\nabla P+\\ \nabla\cdot\overline{\overline{\boldsymbol{\tau}}}_k+\alpha_k\rho_k\boldsymbol{g}+&\sum(\boldsymbol{R}_{pk}+\dot{m}_{pk}\boldsymbol{v}_{pk}-\dot{m}_{kp}\boldsymbol{v}_{kp})+\\ &(\boldsymbol{F}_k+\boldsymbol{F}_{\mathrm{lift},k}+\boldsymbol{F}_{v_{\mathrm{m}},k}),\end{aligned} \quad (2)$$

where $\boldsymbol{F}_k$ is the external volume force, $\boldsymbol{F}_{\mathrm{lift},k}$ is the lift force, $\boldsymbol{F}_{v_{\mathrm{m}},k}$ is the virtual mass force, $\boldsymbol{R}_{pk}$ is the interaction force between p and k phases, P is the pressure shared by all phases, $\boldsymbol{v}_{pk}$ and $\boldsymbol{v}_{kp}$ are phase velocities, $\boldsymbol{g}$ is the gravitational acceleration, and $\overline{\overline{\boldsymbol{\tau}}}_k$ is the pressure strain of the k phase. $\overline{\overline{\boldsymbol{\tau}}}_k$ can be calculated as follows:

$$\overline{\overline{\boldsymbol{\tau}}}_k=\alpha_k\mu_k(\nabla\boldsymbol{v}_k+\nabla\boldsymbol{v}_k^{\mathrm{T}})+\alpha_k\left(\lambda_k-\frac{2}{3}\mu_k\right)(\nabla\cdot\boldsymbol{v}_k)\boldsymbol{I}, \quad (3)$$

where μ_k and λ_k are the shear viscosity coefficient and bulk viscosity coefficient of the k phase, respectively, and $\boldsymbol{I}$ is the unit tensor.

The volume fraction equation for each phase can be obtained from the continuity equation:

$$\frac{1}{\rho_{\mathrm{r}k}}\left[\frac{\partial}{\partial t}(\alpha_k\rho_k)+\nabla\cdot(\alpha_k\rho_k\boldsymbol{v}_k)-\sum(\dot{m}_{pk}-\dot{m}_{kp})\right]=0, \quad (4)$$

where $\rho_{\mathrm{r}k}$ is the phase reference density, that is, the volumetric average density of the k phase.

2.3 Numerical gridding and boundary conditions

The flow channel was discretized using a structured grid division method. Five layers of grids were set in the direction of clearance thickness, 400 layers in the axial direction, and 400 layers in the circumferential direction. The total number of grid cells is approximately 7.2×10^5. For the flow channel model with PEGs, 18 layers of grids were set in the depth and width directions of the PEGs, with the total number of grid cells being approximately 1.03×10^6. The gridding strategy is illustrated in Fig. 2.

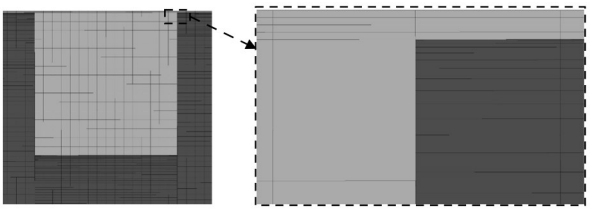

Fig. 2 Structure grid of the flow channel

The medium was a mixture of oil and solids. We set the boundary conditions as a pressure inlet and pressure outlet. The inlet pressure was set at 7 MPa, and the outlet pressure was set to the atmospheric pressure. The first phase is the oil, and we assume the second phase to be comprised of ideal spherical solid particles with a density of ρ=7500 kg/m^3 and a dynamic viscosity of $\mu=1\times10^{-5}$ Pa·s. The solid particle diameters were set to range from 3 to 12 μm. The volume fraction of the inlet particles was set at 3%. In the Euler–Euler model, the drag force function between the solid and liquid phases was selected as Syamlal–O'Brien. In the phase interactions, the drag is selected as Schiller–Naumann, and the lift is selected as "none", meaning there is no separation of phases.

In the present geometric model, the critical Reynolds number of an asymmetric annular clearance with a PEG is the smallest, which is 400. It corresponds to a velocity of 366 mm/s, which is greater than the actual flow velocity of the fit clearance. Therefore, the fluid flow in the clearance is in a laminar state, and the viscous model adopts a laminar model.

In this study, a pressure-based solver was employed for the numerical solution. The gradient was set to be the cell-based least squares method, which is calculated based on the cell center. The pressure, momentum, and turbulence terms were second order upwind with higher accuracy. The discretized control equations are solved using the semi-implicit method for pressure linked equation (SIMPLE) algorithm. In the numerical solution process, we consider that convergence has occurred when the residual of the monitored physical quantity is less than 1×10^{-6}, and the inlet and outlet pressure difference remains constant with fluctuations below 1%.

2.4 Method validation

In order to verify the accuracy of the numerical simulation, a concentric ring clearance model was established. The clearance flow obtained from this

theoretical calculation was compared with that from the numerical calculation. Due to $\delta/D \ll 1$ (δ is the fit clearance between the valve core and sleeve and D is the diameter of the valve core (D=9.6 mm) (Fig. 1)), the flow in the annular clearance can be considered as parallel plate gap flow. According to the principle of clearance flow, the formula for the flow of the concentric ring-shaped clearance between the valve core and the valve body is as follows:

$$Q_{\mathrm{T}} = \frac{\pi D \delta^3 \Delta p}{12 \mu l_1}, \tag{5}$$

where Δp is the pressure difference at the inlet and outlet of the fit clearance (Δp=7 MPa), l_1 is the length of the fit clearance (l_1=10 mm), and μ is the kinematic viscosity.

The flow calculated by theoretical methods was compared with that of the numerical simulation, as shown in Table 1. The maximum error between the theoretical and simulation results is 6.06%, and the fit clearance size is 5 μm. The error generated is within a reasonable range, and thus, the numerical method and results are accurate and reliable.

Table 1 Flow calculated by the theoretical equation (Q_{T}) and the numerical simulation (Q_{S}) at different fit clearances

δ (μm)	Q_{T} (mL/min)	Q_{S} (mL/min)	Error (%)
5	0.33	0.35	6.06
10	2.65	2.73	3.02
15	8.95	9.44	5.47
20	21.22	21.84	2.92

We also conducted experimental verification of the simulation model, with the results shown in Table 2 (Wang et al., 2026). The maximum error between the experimental and simulation results is 8.0%, which is within a reasonable range, indicating that the simulation method is reliable.

Table 2 Comparison of flow rate for the experimental and simulation results. Reprinted from (Wang et al., 2026), Copyrights 2026, with permission from Elsevier

Opening (%)	Flow rate (L/min)		Error (%)
	Experiment	Simulation	
10	3.0	3.1	3.3
30	10.0	9.2	8.0
50	16.0	14.9	6.9
70	19.5	20.2	3.5
90	23.5	25.5	7.8

3 Results and discussion

3.1 Fluid force of the valve core within an asymmetric fit clearance

This section focuses on the fluid force within the asymmetric fit clearance of the valve core. The impact of the inclination angle on the fluid force of the valve core was analyzed. The variation patterns of the fluid dynamics of the valve core with uniform grooves were studied under different inclination angles.

3.1.1 Fluid force analysis without PEG

The flow channel model with an initial fit clearance of 20 μm was selected for analysis. The pressure distribution on the upper and lower surfaces of the valve shoulder (θ=π and θ=0) at different inclination angles is shown in Fig. 3. As shown in Fig. 3a, the pressure distribution on the surface of the valve core shoulder is significantly uneven. At the same axial

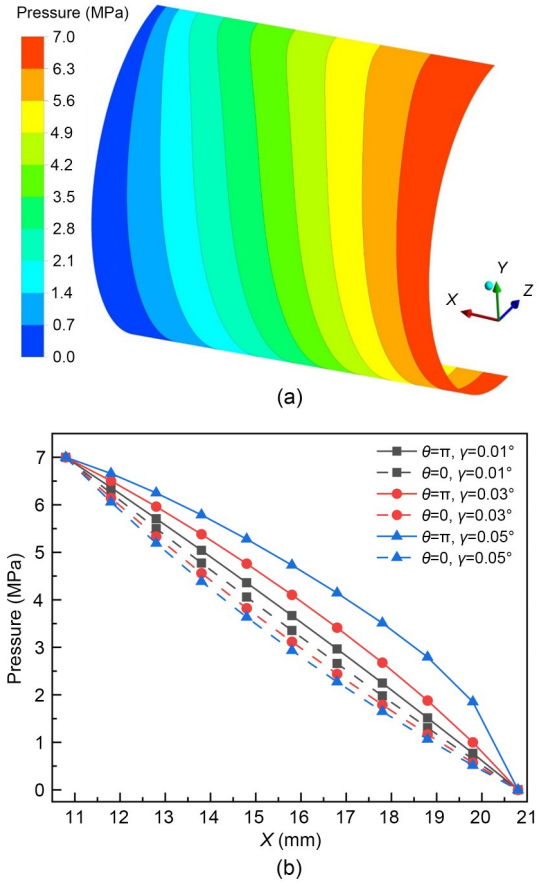

Fig. 3 Pressure of the upper and lower surfaces of the valve core shoulder at different inclination angles: (a) pressure distribution; (b) pressure curves

position, the pressure on the upper surface of the valve core shoulder is higher than that on the lower surface. From Fig. 3b, it is clear that as the inclination angle increases, the pressure on the lower surface of the valve core shoulder decreases, while the pressure on the upper surface increases. In the axial direction, at the same position, the pressure increment on the upper surface is increasing. According to the Bernoulli principle (Li et al., 2021), when the fit clearance size between the upper surface and the valve sleeve is small at the outlet, the speed decreases, and the pressure increases.

Next, the flow channel model with an inclination angle of 0.03° is selected for analysis. Under different valve core shoulder clearance values, the pressure curves of the upper and lower surfaces are shown in Fig. 4. As the clearance increases, the pressure on the upper surface of the valve core shoulder ($\theta=\pi$) decreases, while the pressure on the lower surface ($\theta=0$) increases. This results in a reduction in the radial fluid force acting on the valve core. However, the increased valve core clearance leads to increased leakage. Therefore, it is necessary to comprehensively consider leakage and radial fluid force to achieve optimal design of the valve core clearance.

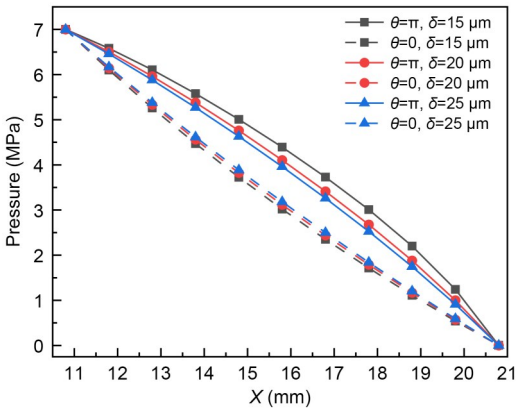

Fig. 4 Pressure curves of the upper and lower surfaces of the valve shoulder for different clearances

The distribution of the pressure difference between the upper and lower surfaces of the valve shoulder under different clearance sizes and inclination angles is shown in Fig. 5. The pressure difference is positively correlated with the inclination angle and negatively correlated with the clearance. The pressure difference with a clearance of 15 μm and an inclination angle of 0.03° is equal to the pressure difference with a clearance of 25 μm and an inclination angle of 0.05°.

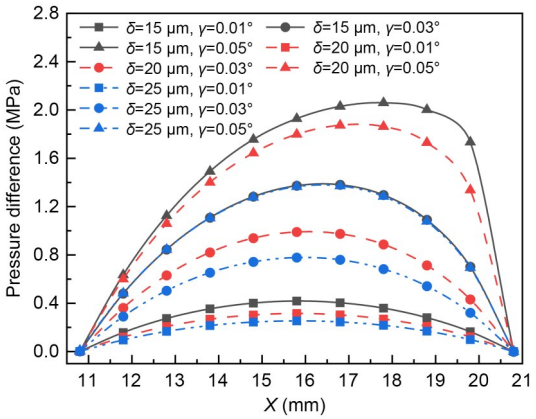

Fig. 5 Pressure difference curves of the upper and lower surfaces

Table 3 shows the radial fluid forces acting on the valve core shoulder within the fit clearance. The radial fluid force increases with the inclination angle and decreases as the fit clearance increases. The increased radial fluid force further increased the inclination of the valve core, making it more prone to contact the valve sleeve, thereby causing sticking problems.

Table 3 Radial fluid force acting on the valve core at different inclinations

Clearance (μm)	Radial fluid force (N)		
	γ=0.01°	γ=0.03°	γ=0.05°
15	21.14	65.76	–
20	15.99	48.75	83.96
25	12.83	38.81	65.23

3.1.2 Fluid force analysis with PEGs

Establishing a PEG on the valve core shoulder is the mainstream improvement measure to overcome the uneven pressure distribution within the fit clearance. Fig. 6 shows the pressure distribution of the valve core shoulder surface with PEGs. The pressure distribution on the upper and lower surfaces of the valve

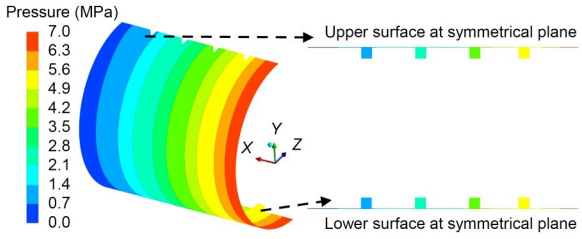

Fig. 6 Pressure distribution of the valve core shoulder surface with PEGs

core shoulder along the circumferential direction is more uniform compared to the case without the PEG in Fig. 3, especially at the position of the PEG. However, in the position without the PEG (inlet and outlet), the fit clearance between the upper and lower surfaces of the valve core shoulder is asymmetrical. Moreover, the pressure on the upper surface at the same position is greater than that on the lower surface. It can thus be concluded that the PEG effectively divides the pressure within the fit clearance into multiple pressure reduction zones.

Fig. 7 presents the pressure curve on the upper and lower surfaces of the valve core shoulder at a clearance of 20 μm and an inclination angle of 0.03°. As seen, the presence of the PEG results in a similar pressure distribution on the upper and lower surfaces of the valve core shoulder. The maximum pressure difference between them occurs at the inlet and is 0.075 MPa. Compared to the case without the PEG, the pressure difference is reduced by a factor of about 100. Meanwhile, the existence of the PEG divides the uneven pressure distribution within the clearance into multiple segments. At the position of the PEG, there is almost no pressure difference.

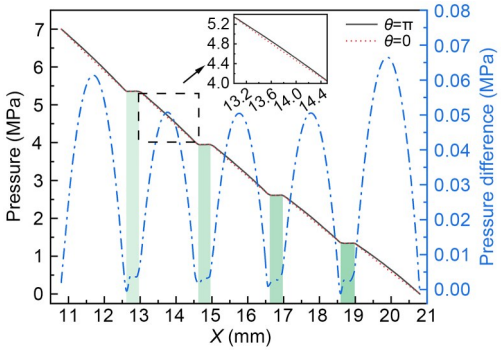

Fig. 7 Pressure curves of the valve core shoulder surface with PEGs at a clearance of 20 μm and an inclination angle of 0.03°

Furthermore, the pressure difference curves of the valve core shoulder surface with PEGs at different inclination angles are shown in Fig. 8. As the inclination angle increases, the pressure difference in the PEG region remains almost unchanged, while the pressure difference in the region without PEG increases. At this point, the pressure difference at the outlet is significantly greater than that at the inlet.

The radial fluid force of the valve core shoulder at a clearance value of 20 μm is shown in Table 4. It

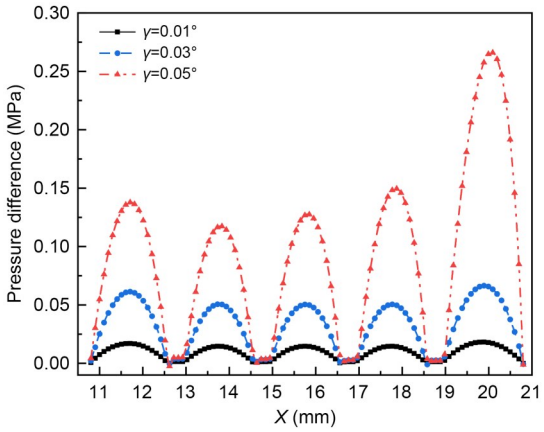

Fig. 8 Pressure difference curves with PEGs at different inclination angles

Table 4 Radial fluid force of the valve core shoulder at different inclination angles

Item	Radial fluid force (N)		
	γ=0.01°	γ=0.03°	γ=0.05°
Without PEG	15.99	48.75	83.96
With PEG	0.70	2.32	5.41

can be seen that the radial fluid force of the valve core shoulder with PEGs is significantly less than that of the valve core shoulder without PEG; the reduction in force was over 93%. This effectively reduced the inclination degree of the valve core.

3.2 Distribution of solid particles within the asymmetric fit clearance

This section focuses on flow characteristics of oil with solid particles within the asymmetric fit clearance. An investigation of the aggregation laws of solid particles under conditions with and without PEGs was performed.

3.2.1 Distribution of solid particles without PEG

The flow channel model at δ=15 μm and γ=0.01° was selected for analysis, and the minimum clearance size was 13.72 μm. The distributions of the particle volume fraction (c) within the fit clearance under different solid particle diameters (d_s) are shown in Fig. 9 when the inlet particle volume fraction (c_0) is 3%. The existence of the valve core inclination angle makes the upper part of the valve core shoulder have a smaller size, resulting in particles accumulating on the lower surface. As the diameter of the solid particles gradually increases, the particle volume fraction is lower in the

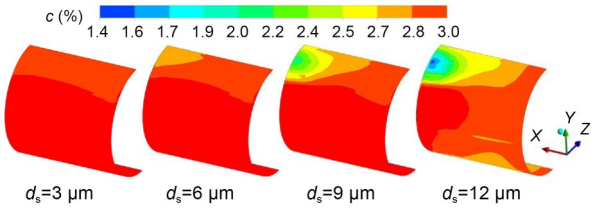

Fig. 9 Distribution of the particle volume fraction (δ=15 μm, γ=0.01°, and c_0=3%)

middle area of the outlet and higher in the surrounding area. This is because the particle diameters gradually approach the clearance size, resulting in a low concentration of particles in the middle area. This is particularly evident when the solid particle diameter is 12 μm, where the minimum particle volume fraction reaches 1.4%.

Similarly, the distribution of the particle volume fraction (c) within the fit clearance at γ=0.03° is depicted in Fig. 10. The minimum clearance size is 8.11 μm. When the particle diameter is greater than 6 μm, particles will aggregate on the upper surface of the valve core shoulder. The volume fraction of particles is approximately 4%, which is greater than the volume fraction of the inlet. Near the minimum fit clearance size, the volume fraction of solid particles is 0. When the particle diameter is greater than the clearance size, the particles will be unable to enter; this is the sensitive sticking area. When solid particles continue to accumulate in the fit clearance, they will seriously hinder the movement of the valve core, resulting in sticking. When the inclination angle is 0.05°, the minimum size of the clearance is 0.85 μm, which is smaller than the particle diameter (therefore, this scenario does not lead to sticking issues).

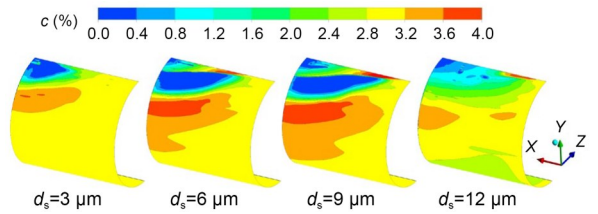

Fig. 10 Distribution of the particle volume fraction (δ=15 μm, γ=0.03°, and c_0=3%)

3.2.2 Distribution of solid particles with PEGs

The distribution of solid particles in the clearance with PEGs at different inclination angles is shown in Fig. 11. Compared with the distribution of solid particles

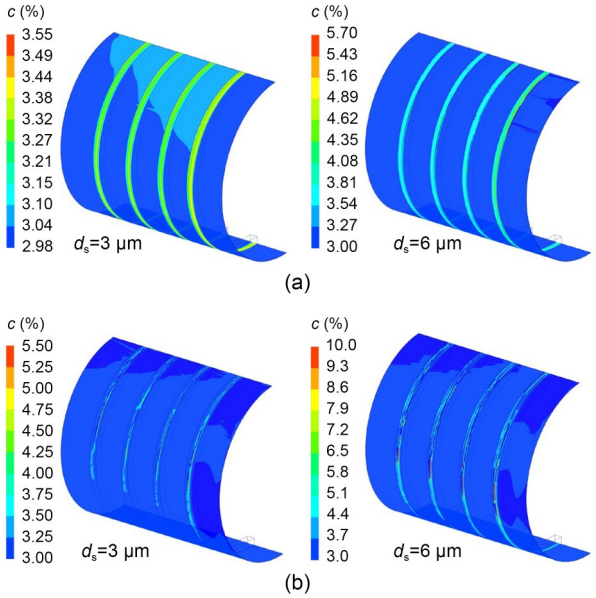

Fig. 11 Distribution of the particle volume fraction with PEGs: (a) γ=0.01°; (b) γ=0.03°

in clearance without PEG, the solid particles are mainly located at the position of the PEG. Moreover, the particle accumulation slows down in the sensitive sticking area. As the size of the solid particles increases, the particle volume fraction at the position of the PEG also increases. When the inclination angle is 0.01°, the maximum particle volume fraction increases from 3.55% at a d_s of 3 μm to 5.70% at a d_s of 6 μm. Varying inclination angles have different effects on the particle aggregation of the PEG. As the inclination angle increases, the clearance size changes, resulting in an increase in the particle volume fraction at the PEG.

3.3 Optimization design of the PEG

Based on the above analysis, the valve shoulder with PEGs can reduce the radial fluid force, as well as decrease the valve core inclination degree. At the same time, it is beneficial to the aggregation of particles in the PEG, indicating that the PEG can effectively reduce the probability of the valve core sticking. In this section, we propose the Tri-PEG. The optimal structural parameters of the Tri-PEG are determined through the response surface analysis method and the multi-objective genetic algorithm.

3.3.1 Optimizing the design of the PEG

Our previous study revealed that the Tri-PEG has a more significant effect on particle retention compared

to uniform rectangular grooves (Hang et al., 2026). It can effectively prevent particles from aggregating in the area without the PEG. Therefore, in order to enhance the dirt-retaining capacity of the PEG and reduce the leakage rate of the clearance, a PEG consisting of a triangular cross-section and an arc-shaped bottom was designed, as shown in Fig. 12. Meanwhile, the structural dimensions of the original valve core shoulder were maintained.

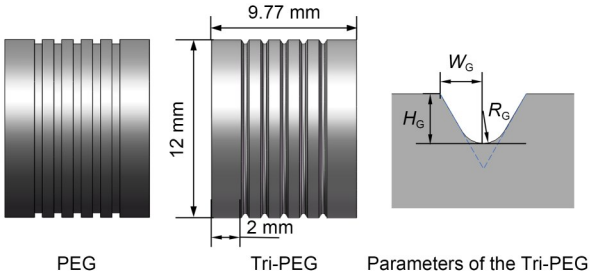

Fig. 12 Structural diagram of Tri-PEG (W_G is the half groove width, H_G is the groove depth, and R_G is the arc-shaped radius)

Response surface methodology (RSM) was used to optimize the structural parameters of the Tri-PEG. The accuracy of the fitted response surface is significantly influenced by the distribution of the test sample points. To ensure that each selected design point is representative and to improve computational efficiency, the Latin hypercube sampling (LHS) method (Aljubran and Horne, 2020) was used to design the test samples. The sample type was central composite design (CCD) sampling, and a total of 15 sets of test design points were generated. The design parameters and results are presented in Tables S1 and S2 of the ESM.

3.3.2 Response surface analysis

The response relationship between the design parameters and the particle volume fraction and the clearance leakage is obtained through fitting of the above simulation data. Fig. 13a shows how the particle volume fraction of the Tri-PEG bottom varies with W_G and H_G at R_G=0.15 mm. The particle volume fraction increases sharply as H_G varies from 0.3 to 0.4 mm, while W_G has little effect on the particle volume fraction. As H_G increases, the volume of the PEG expands, and the residence time of the fluid in the PEG is prolonged, making it easier for particles to be captured by vortices in the groove. However, after H_G reaches a certain value, the flow field inside the groove tends to

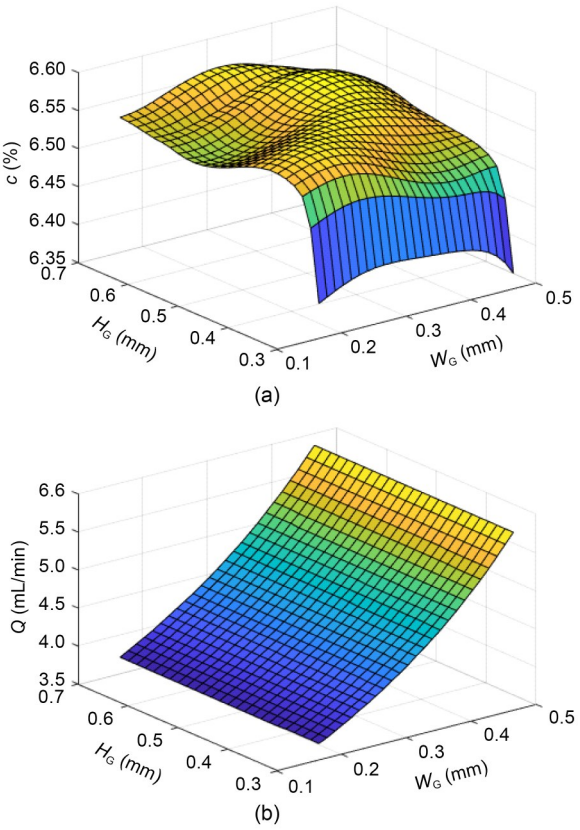

Fig. 13 Variation of (a) particle volume fraction and (b) leakage rate with W_G and H_G (R_G=0.15 mm)

stabilize, and the vortex structure becomes fully developed. Further increasing H_G weakens the effect of particle capture in the groove. Thus, as H_G varies from 0.4 to 0.7 mm, the resulting changes are relatively gentle. At this time, changing W_G will alter the cross-sectional shape of the groove, affecting the secondary flow intensity and the lateral transport of particles and thereby affecting the volume fraction of particles in the groove. As W_G increases, the particle volume fraction first increases and then decreases. When W_G is constant, the effect of H_G on particle concentration slightly differs. When W_G=0.2 mm, the particle volume fraction shows a trend of first increasing, then decreasing, and then increasing again with greater H_G. For W_G= 0.3 mm, the particle volume fraction first increases and then decreases with an increase in H_G, and a maximum value region forms. When W_G=0.45 mm, the particle volume fraction first increases and then stabilizes. From the above, it can be concluded that when H_G and W_G are both set to the middle value, the particle volume fraction at the bottom of Tri-PEG reaches a maximum.

Fig. 13b depicts the leakage rate (Q) of the clearance with Tri-PEG, which varies with W_G and H_G at R_G= 0.15 mm. The leakage rate increases exponentially with W_G, rising from a minimum of 3.52 to 6.00 mL/min. This is because the leakage mainly depends on the axial clearance; as W_G increases, the effective flow area of the fluid leakage increases, making leakage more likely. The effect of H_G on the effective flow area of the fluid leakage is relatively small. Therefore, the impact of H_G on leakage is minor.

Fig. 14a presents how the particle volume fraction of the Tri-PEG bottom varies with W_G and R_G at H_G= 0.5 mm. The particle volume fraction first increases and then decreases with an increase in W_G. When W_G is constant, the particle volume fraction shows a trend of increasing first and then decreasing with greater R_G. This indicates the existence of a critical R_G value, where the flow field and particle dynamics in the groove are optimally matched. When R_G exceeds this critical value, the centrifugal force in the groove weakens, and the ability to capture particles decreases. For R_G in the range of 0.22–0.25 mm, there is an obvious decreasing trend. From these results, we can conclude that when W_G is approximately 0.3 mm and R_G is approximately 0.2 mm, the particle volume fraction reaches its maximum value.

Fig. 14b shows how the leakage rate of the fit clearance for Tri-PEG varies with W_G and R_G at H_G= 0.5 mm. When R_G is constant, the leakage rate increases exponentially as W_G increases, which is consistent with earlier results. When W_G is constant, R_G has a relatively small influence on the leakage rate. Considering these findings, it is clear that the main factor influencing leakage is W_G, while H_G and R_G have a relatively small impact on leakage. Choosing a smaller W_G can thus promote a smaller leakage rate.

Fig. 15a shows how the particle volume fraction of the Tri-PEG bottom varies with H_G and R_G at W_G= 0.315 mm. If R_G is constant, the particle volume fraction first increases and then stabilizes as H_G increases. For H_G in the range of 0.3–0.4 mm, the change in the particle volume fraction is significant; this is consistent with the trend from Fig. 13a. When H_G is 0.3 mm, the effect of R_G on the particle volume fraction is consistent with the above. After H_G exceeds 0.4 mm, the change in particle volume fraction is minimal, indicating that the effects of H_G and R_G on the particle volume fraction cancel each other out. Considering these results, one can conclude that when H_G is approximately 0.4 mm and R_G takes on the middle value, the particle volume fraction reaches a maximum.

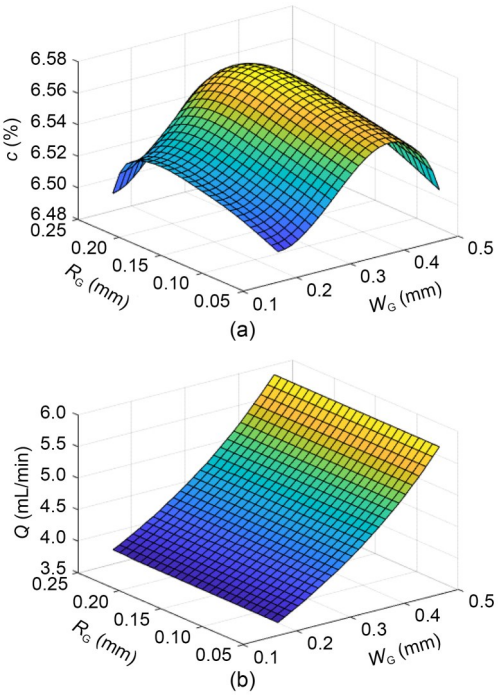

Fig. 14 Variation of (a) particle volume fraction and (b) leakage rate with W_G and R_G (H_G=0.5 mm)

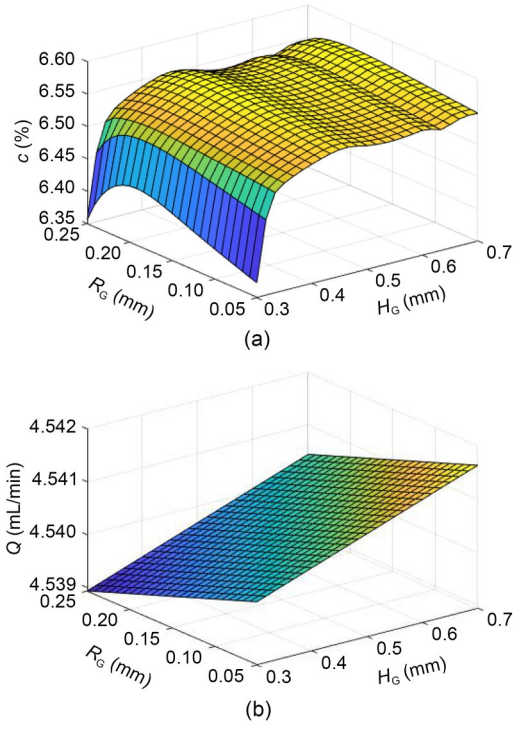

Fig. 15 Variation of (a) particle volume fraction and (b) leakage rate with H_G and R_G (W_G=0.315 mm)

Fig. 15b depicts how the leakage rate of the fit clearance for Tri-PEG varies with H_G and R_G at W_G= 0.315 mm. Clearly, the leakage rate is linearly correlated with R_G or H_G; specifically, the leakage rate is negatively correlated with R_G and positively correlated with H_G. However, the influence of both factors on the leakage rate is very small, varying between 4.534 and 4.546 mL/min. This is consistent with the previous conclusion. From the above, it can be deduced that choosing a smaller H_G and a larger R_G can minimize the leakage.

3.3.3 Determination of the parameters of the PEG

The optimization objective is to minimize the leakage and maximize the particle volume fraction at the Tri-PEG. The influence of the design parameters on the leakage and the particle volume fraction exhibits different positive and negative correlations. Therefore, a multi-objective genetic algorithm was employed to balance the optimal solutions among various responses and find the Pareto solution (Deb et al., 2002). The optimized parameter values of the Tri-PEG structures obtained from this approach are shown in Table 5. Compared with the rectangular PEG structure, the optimal parameter combination of the Tri-PEG reduces the leakage rate by 12% and increases the particle volume fraction by 6%. Therefore, the optimized Tri-PEG structure can control the leakage rate of the fit clearance and the degree of dirt accumulation at the bottom of the groove. Accordingly, it can reduce the possibility of hydraulic spool valve sticking.

Table 5 Results of the multi-objective optimization

Parameter	Value		Variation
	PEG	Tri-PEG	
W_G (mm)	0.265	0.215	–
H_G (mm)	0.300	0.392	–
R_G (mm)	–	0.200	–
Q (mL/min)	4.260	3.760	−12%
c (%)	6.270	6.650	6%

4 Conclusions

This study involved a systematic investigation of the mechanism of valve core sticking formation from the perspective of the unbalanced radial force and solid particle intrusion into the fit clearance. The effects of inclination angle, clearance size, and particle diameter were analyzed. We proposed a novel PEG structure and further adopted multi-objective optimization to obtain optimal structural parameters.

Through simulations, it was revealed that the radial fluid force is positively correlated with the inclination angle and negatively correlated with the clearance. When the particle diameter reaches a certain value, the volume fraction of solid particles in the sensitive sticking area is relatively small. The introduction of PEG into the valve core is beneficial for reducing the uneven distribution of pressure in the fit clearance and can slow down the aggregation of particles in the sensitive sticking area. The particles are mainly concentrated in the PEG, which helps to reduce the occurrence of valve core sticking.

The W_G of the Tri-PEG was revealed to be the main factor affecting the leakage at the fit clearance. The H_G and R_G have positive and negative effects on the leakage rate, respectively, but their impacts are relatively small. Compared with the rectangular PEG structure, the optimal Tri-PEG structure reduces the leakage rate by 12% and increases the volume fraction of particles in the groove by 6%. It can therefore control the leakage at the valve core clearance and the degree of particle concentration at the bottom of the groove.

Moreover, the optimized Tri-PEG structure effectively reduces the unbalanced radial force by homogenizing the pressure distribution in the fit clearance while simultaneously acting as an efficient particle trap to mitigate sticking risk. However, it should be noted that the optimization results and conclusions of this study were obtained under specific simulation operating conditions. If there are significant changes in the working fluid and operating conditions, then the optimal structural parameters of the Tri-PEG structure may change.

Acknowledgments

This work is supported by the National Natural Science Foundation of China (No. 52422506), the Priority-Funded Postdoctoral Research Project, Zhejiang Province (No. ZJ2025205), and the Zhejiang Key Research and Development Project (No. 2024C01235), China.

Author contributions

Zhen-hao LIN designed the research and processed the corresponding data. Zhen-hao LIN, Yu-wei WANG, and Zhe-hui MA wrote the first draft of the manuscript. Tian-xiao ZHANG helped to organize the manuscript. Zhi-jiang JIN and Jin-yuan QIAN revised and edited the final version.

Conflict of interest

Zhen-hao LIN, Yu-wei WANG, Zhe-hui MA, Tian-xiao ZHANG, Zhi-jiang JIN, and Jin-yuan QIAN declare that they have no conflict of interest.

References

Aljubran M, Horne R, 2020. Prediction of multilateral inflow control valve flow performance using machine learning. *SPE Production & Operations*, 35(3):691-702. https://doi.org/10.2118/196003-PA

Amirante R, Distaso E, Tamburrano P, 2016. Sliding spool design for reducing the actuation forces in direct operated proportional directional valves: experimental validation. *Energy Conversion and Management*, 119:399-410. https://doi.org/10.1016/j.enconman.2016.04.068

Chen QP, Liu M, Ji H, et al., 2024. Characterization of hydraulic spool clamping triggered by solid particles based on mechanical model and experiment research. *Applied Sciences*, 14(19):8880. https://doi.org/10.3390/app14198880

Chu YB, Yuan ZH, He XG, et al., 2021. Model construction and performance degradation characteristics of a deflector jet pressure servo valve under the condition of oil contamination. *International Journal of Aerospace Engineering*, 2021:8840084. https://doi.org/10.1155/2021/8840084

Deb K, Pratap A, Agarwal S, et al., 2002. A fast and elitist multiobjective genetic algorithm: NSGA-II. *IEEE Transactions on Evolutionary Computation*, 6(2):182-197. https://doi.org/10.1109/4235.996017

Deng WX, Zhou H, Zhou J, et al., 2023. Neural network-based adaptive asymptotic prescribed performance tracking control of hydraulic manipulators. *IEEE Transactions on Systems, Man, and Cybernetics: Systems*, 53(1):285-295. https://doi.org/10.1109/tsmc.2022.3178626

Domagała M, Momeni H, Domagala-Fabis J, et al., 2018. Simulation of particle erosion in a hydraulic valve. *Materials Research Proceedings*, 5:17-24. https://doi.org/10.21741/9781945291814-4

Gao ZX, Liu P, Yue Y, et al., 2020. Comparison of swing and tilting check valves flowing compressible fluids. *Micromachines*, 11(8):758. https://doi.org/10.3390/mi11080758

Gui SY, Zhang SS, Fu B, et al., 2022. Fluid-dynamic analysis and multi-objective design optimization of piezoelectric servo valves. *Flow Measurement and Instrumentation*, 85:102157. https://doi.org/10.1016/j.flowmeasinst.2022.102157

Hang LF, Guan AQ, Gu XJ, et al., 2026. Effects of throttle groove on viscous heating and thermal deformation of spool valve core. *Aerospace Science and Technology*, 168:110744. https://doi.org/10.1016/j.ast.2025.110744

Hong SH, Kim KW, 2016. A new type groove for hydraulic spool valve. *Tribology International*, 103:629-640. https://doi.org/10.1016/j.triboint.2016.07.009

Hou FW, Shu HF, Wu BB, et al., 2025. Parametric design for the valve seat of a high-temperature and high-pressure valve inside wind tunnels. *Journal of Zhejiang University-SCIENCE A*, 26(3):266-276. https://doi.org/10.1631/jzus.A2300546

Jiang JH, Duan BS, Zhang J, et al., 2019. The influence of pressure difference at the valve port of hydraulic throttle cone valve on the luminescence of hydraulic oil. *International Journal of Hydromechatronics*, 2(2):140-156. https://doi.org/10.1504/ijhm.2019.100771

Li HY, Liu JK, Li K, et al., 2021. Development of a high differential pressure piezoelectric active proportional regulation valve using a bending transducer. *IEEE Transactions on Industrial Electronics*, 68(12):12513-12523. https://doi.org/10.1109/tie.2020.3044814

Li LZ, Zhang YP, Tian WX, et al., 2014. MAAP5 simulation of the PWR severe accident induced by pressurizer safety valve stuck-open accident. *Progress in Nuclear Energy*, 77:141-151. https://doi.org/10.1016/j.pnucene.2014.06.014

Li RC, Sun YH, Wu XW, et al., 2023. Review of the research on and optimization of the flow force of hydraulic spool valves. *Processes*, 11(7):2183. https://doi.org/10.3390/pr11072183

Li WD, Jiang HP, Feng CH, et al., 2025. A hybrid intelligent diagnostic approach for spool jamming faults of hydraulic directional valves. *Measurement*, 241:115706. https://doi.org/10.1016/j.measurement.2024.115706

Lisowski E, Filo G, Rajda J, 2018. Analysis of flow forces in the initial phase of throttle gap opening in a proportional control valve. *Flow Measurement and Instrumentation*, 59:157-167. https://doi.org/10.1016/j.flowmeasinst.2017.12.011

Liu XQ, Ji H, Min W, et al., 2020. Erosion behavior and influence of solid particles in hydraulic spool valve without notches. *Engineering Failure Analysis*, 108:104262. https://doi.org/10.1016/j.engfailanal.2019.104262

Lu L, Wang J, Li MR, et al., 2022. Experimental and numerical analysis on vortex cavitation morphological characteristics in U-shape notch spool valve and the vortex cavitation coupled choked flow conditions. *International Journal of Heat and Mass Transfer*, 189:122707. https://doi.org/10.1016/j.ijheatmasstransfer.2022.122707

Mittal R, Iaccarino G, 2005. Immersed boundary methods. *Annual Review of Fluid Mechanics*, 37:239-261. https://doi.org/10.1146/annurev.fluid.37.061903.175743

Qian JY, Liu BZ, Lei LN, et al., 2016. Effects of orifice on pressure difference in pilot-control globe valve by experimental and numerical methods. *International Journal of Hydrogen Energy*, 41(41):18562-18570. https://doi.org/10.1016/j.ijhydene.2016.08.070

Qian JY, Mu J, Hou CW, et al., 2021. A parametric study on unbalanced moment of piston type valve core. *Journal of Zhejiang University-SCIENCE A*, 22(4):265-276. https://doi.org/10.1631/jzus.A2000582

Qian JY, Xu JX, Zhong FP, et al., 2023. Solid-liquid flow characteristics and sticking-force analysis of valve-core fitting clearance. *Journal of Zhejiang University-SCIENCE A*, 24(12):1096-1105.

https://doi.org/10.1631/jzus.A2300061

Shanbhag VV, Meyer TJJ, Caspers LW, et al., 2021. Failure monitoring and predictive maintenance of hydraulic cylinder—state-of-the-art review. *IEEE/ASME Transactions on Mechatronics*, 26(6):3087-3103. https://doi.org/10.1109/tmech.2021.3053173

Shi X, Chai YY, Chen H, et al., 2024. Numerical simulation of pressure loss and flow characteristics in combined elbow pipes for solid-liquid two-phase flow. *Water Science & Technology*, 90(4):1099-1114. https://doi.org/10.2166/wst.2024.262

Sun F, Xu H, Cheng M, et al., 2021. Sensitive monitoring particles conveying in water hydraulic system via a facile molding conductive hydrogel. *IEEE Sensors Journal*, 21(9): 10506-10513. https://doi.org/10.1109/jsen.2021.3061132

Sun ZC, An T, Qian ZL, et al., 2026. Reliability of valves in nuclear power plant: a review of full life-cycle frameworks and evolution toward physics-data fusion. *Journal of Reliability Science and Engineering*, 2(1):012001. https://doi.org/10.1088/3050-2454/ae4be0

Terrell EJ, Higgs III CF, 2007. A modeling approach for predicting the abrasive particle motion during chemical mechanical polishing. *Journal of Tribology*, 129(4):933-941. https://doi.org/10.1115/1.2768614

Wang GM, Xue LJ, Zhu YF, et al., 2023. Fault diagnosis of power-shift system in continuously variable transmission tractors based on improved echo state network. *Engineering Applications of Artificial Intelligence*, 126:106852. https://doi.org/10.1016/j.engappai.2023.106852

Wang ZT, Li WQ, Wang XH, et al., 2026. Design of asymmetric combined flow-guiding valve core structure in hydraulic spool valve. *Annals of Nuclear Energy*, 227:11938. https://doi.org/10.1016/j.anucene.2025.111938

Yin YB, Yuan JY, Guo SR, 2017. Numerical study of solid particle erosion in hydraulic spool valves. *Wear*, 392-393: 174-189. https://doi.org/10.1016/j.wear.2017.09.021

Zhang J, Du RH, Dong PP, et al., 2025. Effect of slide valve gap surface roughness on particle transport properties. *Aerospace*, 12(7):608. https://doi.org/10.3390/aerospace12070608

Zhang SZ, Lin ZH, Chen SJ, et al., 2024. Unbalanced force analysis on valve core clamping in hydraulic spool valves. *Annals of Nuclear Energy*, 203:110505. https://doi.org/10.1016/j.anucene.2024.110505

Zhang XL, Wang AL, Chen W, et al., 2020. Methodology for expressing the flow coefficients of coupled throttling grooves in a proportional—directional valve. *Journal of Zhejiang University-SCIENCE A*, 21(10):799-816. https://doi.org/10.1631/jzus.A1900656

Zhang YH, Ding BC, Zheng SP, et al., 2025. Radial flow force reduction in a hydraulic spool valve using balanced through-hole design. *Physics of Fluids*, 37(9):095114. https://doi.org/10.1063/5.0287141

Zhao RH, Liao YY, Lian ZS, et al., 2021. Research on the performance of a novel electro-hydraulic proportional directional valve with position-feedback groove. *Proceedings of the Institution of Mechanical Engineers, Part E: Journal of Process Mechanical Engineering*, 235(6):1930-1944. https://doi.org/10.1177/09544089211024424

Zheng N, Tong BH, Yang W, et al., 2020. Study on pressure balance and clearance flow characteristics of composite-grooved piston–copper pair. *Journal of the Brazilian Society of Mechanical Sciences and Engineering*, 42(6):286. https://doi.org/10.1007/s40430-020-02353-y

Zhong Q, Bao HM, Li YB, et al., 2021. Investigation into the independent metering control performance of a twin spools valve with switching technology-controlled pilot stage. *Chinese Journal of Mechanical Engineering*, 34(1): 91. https://doi.org/10.1186/s10033-021-00616-w

Zhu XG, Liu PF, Luan JH, et al., 2026. Key technologies and engineering applications of digital simulation for reliability of aerospace products. *Journal of Reliability Science and Engineering*, 2(1):015201. https://doi.org/10.1088/3050-2454/ae3c13

Electronic supplementary materials

Figs. S1 and S2; Tables S1 and S2